Biosensors and Bioelectronics 186 (2021) 113305

Contents lists available at ScienceDirect

Biosensors and Bioelectronics

journal homepage: www.elsevier.com/locate/bios

DNA walker-mediated biosensor for target-triggered triple-mode detection of *Vibrio parahaemolyticus*

Wenting Wei, Han Lin *, Tingting Hao, Sui Wang, Yufang Hu, Zhiyong Guo **, Xingyu Luo

State Key Laboratory for Managing Biotic and Chemical Threats to the Quality and Safety of Agro-products, State Key Laboratory Base of Novel Functional Materials and Preparation Science, School of Materials Science and Chemical Engineering, Ningbo University, Ningbo, 315211, PR China

ARTICLE INFO

Keywords:
Triple signal outputs mode immunosensor
Electrochemiluminescence
Fast scan voltammetry
Fluorescent pixel counting
Pathogenic bacteria
DNA walker

ABSTRACT

Herein, we have constructed a target-triggered and DNA walker-mediated biosensor with triple signal (BTS) outputs mode for sensitive and reliable detection of pathogenic bacteria. *Vibrio parahaemolyticus* (VP) being the detection target model, the aptamer conformational changes induced by VP have been designed to activate the DNA walk on the modifiable and conductive surface of Fe_3O_4 nanoparticles to generate triple signal outputs, including electrochemiluminescence (ECL), fast scan cyclic voltammetry (FSCV) and fluorescent pixel counting (FLPC). Limits of quantification (LOQ) of VP were as low as 1 CFU·mL^{-1} by ECL with a linear range of 1–10^6 CFU·mL^{-1}, 1 CFU·mL^{-1} by FSCV with a linear range of 1–10^6 CFU·mL^{-1}, and 10 CFU·mL^{-1} by FLPC with a linear range of 10–10^7 CFU·mL^{-1} respectively, all squared correlation coefficients R^2 being > 0.99. In addition, optical and electrochemical results, signal-on and signal-off results, electrode phase and solution phase results could be mutually verified by integrating of multiple detection techniques in one biosensor, greatly improving the accuracy and reliability. Therefore, the designed BTS has provided a powerful strategy for pathogenic bacteria detection considering its high detection sensitivity and accuracy, exhibiting great potential in food safety, water quality and biological contamination.

1. Introduction

Pathogenic bacteria detection is essential in human healthcare precautions (Chen et al., 2017; Yoo and Lee, 2016). In particular, many Gram-negative bacteria (GNB), including *Vibrio parahaemolyticus* (VP), *Vibro cholerae* (VC) and *Yersinia pestis* (YP) have caused different pathogenic and lethiferous risks in human hosts (Costa et al., 2015; Peleg and Hooper, 2010). For instance, VP is one of the representative Gram-negative bacteria that commonly contaminates marine organisms, especially shellfish, and it is considered as a major cause of human gastrointestinal diseases by insecure food intaking (Su and Liu, 2007; Yeung and Boor, 2004; Zhang and Orth, 2013). Gradually, analytical methods based on immunoassay such as enzyme-linked immune-sorbent assay (ELISA) or based on nucleic acids amplification techniques including loop-mediated isothermal amplification (LAMP), and polymerase chain reaction (PCR) have been developed to realize the pathogenic bacteria detection (Azizi et al., 2019; Charlermroj et al., 2014; Hillman et al., 2021; Tlili et al., 2013). However, the single signal output generated by complicated reactions of these methods still remains a notable challenge in suffering from the influences of inherent method limitations, and background signals or even false signals (Gahlaut et al., 2019; Guo et al., 2018; Hao et al., 2020; Wei et al., 2020). Therefore, there is an urgent need to develop a more reliable, accurate and simple strategy for pathogenic bacteria analysis.

Previously, our group has developed a novel method named fast scan anodic stripping voltammetry (FSASV) for sensitive detection of VP by increasing the scan rate of a potential window to amplify electrochemical signals (Wang et al., 2020b). Besides, an aptasensor has also been designed to achieve a dual-mode detection of VP by electrochemiluminescence (ECL) and differential pulse voltammetry (DPV) (Wei et al., 2020). Undoubtedly, multiple detection modes are necessary, because different methods have their own advantages and characteristics, together with respective shortcomings and background interferences. For example, electrochemical methods are simple, fast and sensitive, but they are affected by not only unknown redox substances in the sample which can directly distort the signal, but also unknown impurities which might contaminate the electrode surface to change the signal generation (Zhang et al., 2019). Optical methods are

* Corresponding author.
** Corresponding author.
E-mail addresses: han@poly.es.hokudai.ac.jp (H. Lin), guozhiyong@nbu.edu.cn (Z. Guo).

https://doi.org/10.1016/j.bios.2021.113305
Received 14 April 2021; Received in revised form 27 April 2021; Accepted 2 May 2021
Available online 7 May 2021

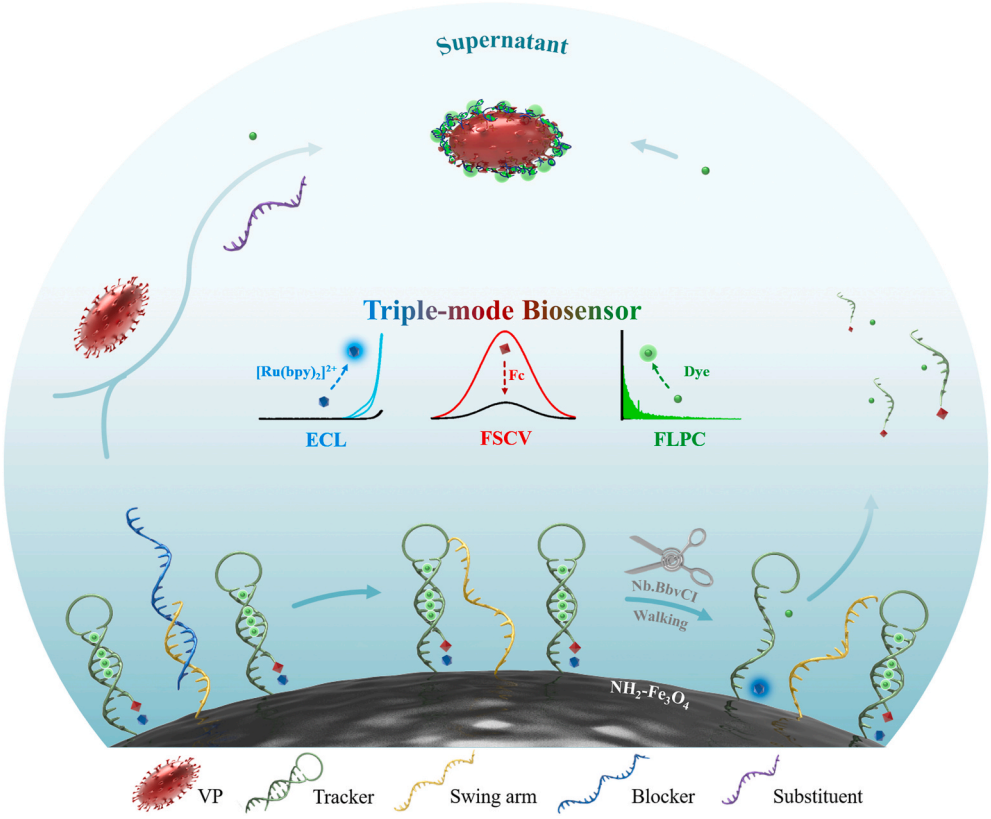

Scheme 1. Schematic illustration of the BTS biosensor with triple signal outputs mode for VP detection based on the activation of DNA strands displacement reactions and endonuclease cleavage of DNA walker.

sensitive, rapid and convenient, but they are interfered by background stray light or luminescent impurities in the sample, environment, reagents and containers (Tagit and Hildebrandt, 2017). Imaging methods are intuitively visible, but the accurate quantification is difficult and the sensitivity is not so good (Smith and Gambhir, 2017). Therefore, using multiple detection modes for the same sample is helpful to avoid respective shortcomings, verify each other, and improve the detection accuracy and reliability (Li et al., 2016). It is worth noting that, multiple detection modes should be not measuring several copies of the same sample with different detection methods, but detecting the same sample through different signals synchronously triggered by the target. In this case, multiple signals can be compared with each other, eliminating the unreliability caused by a single method and the inaccuracy caused by pretreatment of black box samples. Building on those existing advantages, it is appropriate to develop a detection sensor with multiple signal outputs mode to deal with the more complicated bacteria environments and obtain better detection accuracy. Therefore, a rational design strategy and programmable signals generation in the detection sensor are demanded to overcome the challenges in tuning the multiple signal outputs.

Recently, DNA nanomachines based on the Watson-Crick base pairing principle and nuclease assistance have been emerged as powerful tools in biosensing, cellular imaging and drug delivery (Bath and Turberfield, 2007; Hu et al., 2019; Liang et al., 2017; Xiong et al., 2020). With the programmable and autonomous conformational sequence change and signals transfer, various DNA nanomachines including DNA walkers, DNA motors, DNA tweezers and DNA switches are presented with excellent applications in different research fields (Bazrafshan et al., 2020; Pan et al., 2017; Wang et al., 2015, 2021; Zhou et al., 2020). Especially, DNA walkers are well designed to show great potential in efficient signals amplification and controllable monitoring through the signal outputs initiation and accumulation (Lv et al., 2020; Wang et al., 2017). Generally, the constructions of DNA walkers are mostly assisted by nanomaterials with certain structures to support the controllable DNA migration, including gold nanoparticles, carbon nanotubes, and other microparticles which exhibit the properties of high specific surface area and modifiable surface for high DNA loading rate. These nanomaterials were also synthesized as the tracks for improving the sensitivity, accuracy and continuity of DNA directional movement (Hu et al., 2020; Mason et al., 2018). Therefore, a biosensor with a rational design of dynamic DNA nanomachines will be a promising analytical device for accurate and reliable pathogenic bacteria detection.

Herein, as proof of concept, we have developed a biosensor with triple signal outputs mode (BTS) for ultra-sensitive detection and in situ imaging of pathogenic bacteria VP that was constructed based on the nanomaterial Fe_3O_4 nanoparticles and VP aptamer involved DNA walker. As shown in Scheme 1, the surface of Fe_3O_4 nanoparticles is prepared for loading the DNA walker, and its high electrical conductivity can improve the electronic signal transmission and amplification when well-assembled onto the electrode surface. In presence of both the target VP and the substituent, the aptamer fragment of the blocker specifically binds to the VP by hydrogen bonding, van der Waals force, and base pair stacking effect or shape matching. Subsequently, the blocker is reintegrated by folding and shortening its base sequence to highly match the base site of the substituent, which triggers a DNA substitution reaction to form the substituent/blocker duplex. And, the released swing arm performs DNA walking under the action of Nb.BbvCI. During the DNA walking, the signal outputs generated in triple-mode can be detected via the rational combination of ECL signal of Ru(bpy)$_2^{2+}$, fast scan cyclic voltammetric (FSCV) signal of ferrocene (Fc) and fluorescent pixel counting (FLPC) signal of LC green plus, respectively. Above all, ECL and FSCV have been widely demonstrated to contribute to reduce the background signals and increase the detection sensitivity among the electrochemical methods, so that these strategies

are also expected to show the potential of precisely reflecting the transformation of signals during DNA walk (Chen et al., 2019; Kannan et al., 2019; Ma et al., 2020; Wang et al., 2020a, 2020b). Meanwhile, as a digital bioassay, FLPC method can significantly improve the reliability of target detection by scientifically imaging and recording positive fluorescent signals (Zhu et al., 2018). More important, optical and electrochemical results, signal-on and signal-off results, electrode phase and solution phase results could be mutually verified by integrating of multiple detection techniques in one biosensor, further improving the accuracy and reliability. Thence, it is believed that BTS allows to efficiently increase the detection sensitivity and reliability of pathogenic bacteria, thereby providing a more reliable biosensor for bacteriological research and practical sample analysis.

2. Materials and methods

2.1. Materials

All the DNA oligomers in Table S1 were synthesized by Sangon Biotech Co., Ltd. (Shanghai, China). Nb.BbvCI (1000 U·mL^{-1}) was purchased from New England Biolabs (Ipswich, MA, USA). Bis(2,2′-bipyridine)-(5-amino-phenanthroline)ruthenium bis(hexafluorophosphate) ($Ru(bpy)_2(phen\text{-}5\text{-}NH_2)(PF_6)_2$, $Ru(bpy)_2^{2+}$) was purchased from Suna Tech Inc. (Suzhou, China). LC Green plus was purchased from BioFire Diagnostic, Inc. (Salt Lake, UT, USA). Glutaraldehyde, tripropylamine (TPrA) and (3-aminopropyl)triethoxysilane (APTES) were purchased from Alfa Aesar Chemical Co., Ltd. (Shanghai, China). Ethylene diamine tetraacetic acid (EDTA) was purchased from Sigma-Aldrich (St. Louis, MO, USA). Ammonium acetate, sodium citrate, $MgCl_2{\cdot}6H_2O$ and $FeCl_3{\cdot}6H_2O$ were purchased from Sinopharm Chemical Reagent Co., Ltd. (Shanghai, China). VP was obtained from Marine Culture Collection of China (Xiamen, China). A 40 mmol·L^{-1} tris(hydroxyl-methyl)aminomethane-HCl (Tris-HCl) containing 2 mmol·L^{-1} EDTA and 12.5 mmol·L^{-1} $MgCl_2{\cdot}6H_2O$ (pH = 8) was prepared as oligonucleotide stock solution and DNA hybridization solution.

2.2. Instruments

Particle size distribution analysis was acquired using a Malvern Zana ZS 90 Mastersizer (Malvern, UK). Cyclic voltammetry (CV), electrochemical impedance spectroscopy (EIS) and chronocoulometry (CC) were measured on a CHI 660E electrochemistry workstation (CH Instruments, Shanghai, China). ECL tests were performed using a custom-built equipment mainly composed of a CHI 1100A electrochemical workstation (CH Instruments, Shanghai, China) and a BPCL ultra-weak chemiluminescence analyzer (Institute of Biophysics, Chinese Academy of Sciences, Beijing, China). FSCV was carried out on a self-established system including an AFG3021B arbitrary/function generator (Tektronix, Oregon, USA), a TBS1102 digital oscilloscope (Tektronix, Oregon, USA) and a fast scan circuit designed and developed by ourselves (Chen et al., 2019). DNA hybridization and annealing were obtained on T100™ Thermal Cycler PCR instrument (Bio-Rad, Hercules, CA, USA). Imagines of the bacterial cells were taken on a Leica TCS SP5 confocal laser microscope (Leica, Heidelberg, Germany). Polyacrylamide gel electrophoresis (PAGE) images were scanned by a ChemiDoc™ MP System (Bio-Rad, Hercules, CA, USA). A conventional three-electrode system was adopted, using a magnetic glassy carbon electrode (MGCE, 3 mm diameter, Gaoss Union, Wuhan, China) as a working electrode, a platinum wire as a counter electrode and an Ag/AgCl (3 mol L^{-1} KCl) electrode as a reference electrode.

2.3. Preparation of amino functionalized Fe_3O_4 nanoparticles

The synthesis of Fe_3O_4 nanoparticles used the previously reported method with appropriate modifications (Shao et al., 2019). About 2.7 g of $FeCl_3{\cdot}6H_2O$, 7.7 g of NH_4Ac and 0.8 g of sodium citrate were added into 140 mL of ethylene glycol. After vigorous stirring at 160 °C under the nitrogen atmosphere, the mixture solution was transferred into a stainless-steel autoclave lined with PTFE and heated to 200 °C and then kept for 16 h. After magnetically cleaned, Fe_3O_4 nanoparticles were dispersed into 50 mL of ethanol together with 1 mL of APTES, ultrasonicated for 1 h, stirred at room temperature for 6 h, magnetically cleaned and redispersed into 20 mL of water to obtain amino-functionalized Fe_3O_4 nanoparticles (NH_2–Fe_3O_4) dispersion.

2.4. Construction of the DNA walker substrate

The hybridization reaction between swing arm and blocker was performed in DNA hybridization solution by using the PCR instrument to form swing arm/blocker duplex. Besides, a 500 μL of 5 μmol·L^{-1} DNA hairpin structure of the tracker was prepared by annealing in PCR instrument, and then 2 μL of 5 mmol·L^{-1} LC Green plus was added and embedded into the groove of the tracker. Next, 20 μL of 5 mmol·L^{-1} $Ru(bpy)_2^{2+}$, 100 μL of 5 μmol·L^{-1} NH_2-modified swing arm/blocker duplex, 500 μL of 5 μmol·L^{-1} NH_2-modified tracker embedded by LC Green plus and 200 μL of 2.5 wt% glutaraldehyde were successively added into 2 mL of NH_2–Fe_3O_4 nanoparticles dispersion, and incubated at room temperature for 2 h, followed by washing with 40 mmol·L^{-1} Tris-HCl. After redispersed in 2 mL of Tris-HCl, NH_2–Fe_3O_4 nanoparticles multi-functionalized by $Ru(bpy)_2^{2+}$, swing arm/blocker duplex and hairpin tracker were achieved to serve as the DNA walker substrate.

2.5. Bacterial strain and samples preparation

During the VP culture process, about 0.9 g of nutrient broth was dissolved in 50 mL of water and autoclaved for 15 min at 121 °C for preparation of culture medium. Next, the VP strains were added onto the culture medium and incubated in a constant-velocity shaker for 24 h shaking at 28 °C. Then the mixture was centrifuged at 5000 rpm for 5 min to isolate the VP strain from the culture medium solution, which was resuspended in 0.01 mol·L^{-1} pH = 7.4 phosphate buffer saline (PBS). The concentration of VP strain was adjusted to 1.0 × 10^8 CFU·mL^{-1} by UV–Vis absorbance value at 600 nm ($OD_{600\ nm}$ = 1.000). By stepwise dilution, a series of bacterial solutions at the concentration of 10^7, 10^6, 10^5, 10^4, 10^3, 10^2, 10 and 1 CFU·mL^{-1} were obtained. For real samples detection, the seawater samples were collected from East China Sea for direct analysis.

2.6. Triple-mode analysis of VP

A 10 μL of 5 μmol·L^{-1} substituent, 20 μL of the sample containing target VP at different concentrations and 0.2 μL of 10 U·μL^{-1} Nb.BbvCI activated by 1 μL cutsmart were both incubated with 200 μL of the DNA walker substrate at 37 °C for 2 h. Then, the reacted DNA walker substrate was separated and dropped on the surface of MGCE for FSCV and ECL detection. The ECL measurement was performed from 0 to 1.2 V in 0.1 mol·L^{-1} pH = 8.0 Tris-HCl containing 30 mmol·L^{-1} TPrA by using CV methods at a scan rate of 50 mV·s^{-1}. FSCV measurement was carried out in 0.1 mol·L^{-1} pH = 5.5 acetate buffer (HAc-NaAc), with a potential range from −0.4 to 0.8 V, and a scan rate of 1200 V·s^{-1}. Glass slide and 24 mm * 24 mm cover glass with 10 μL sample were placed onto a 20 × 0.7 objective and excited with the 458 nm argon-ion laser. For LC green plus pixels counting, all fluorescence con-focal microscope images were captured and processed into the size of 775 μm * 775 μm with the format of 1024 * 1024 pixels. All images were digitized and counted by self-made program in MATLAB.

3. Results and Discussion

3.1. Construction and characterization of BTS

To achieve the properties of high-density DNA loading, easy separation and rapid preparation of BTS, Fe_3O_4 nanoparticles were

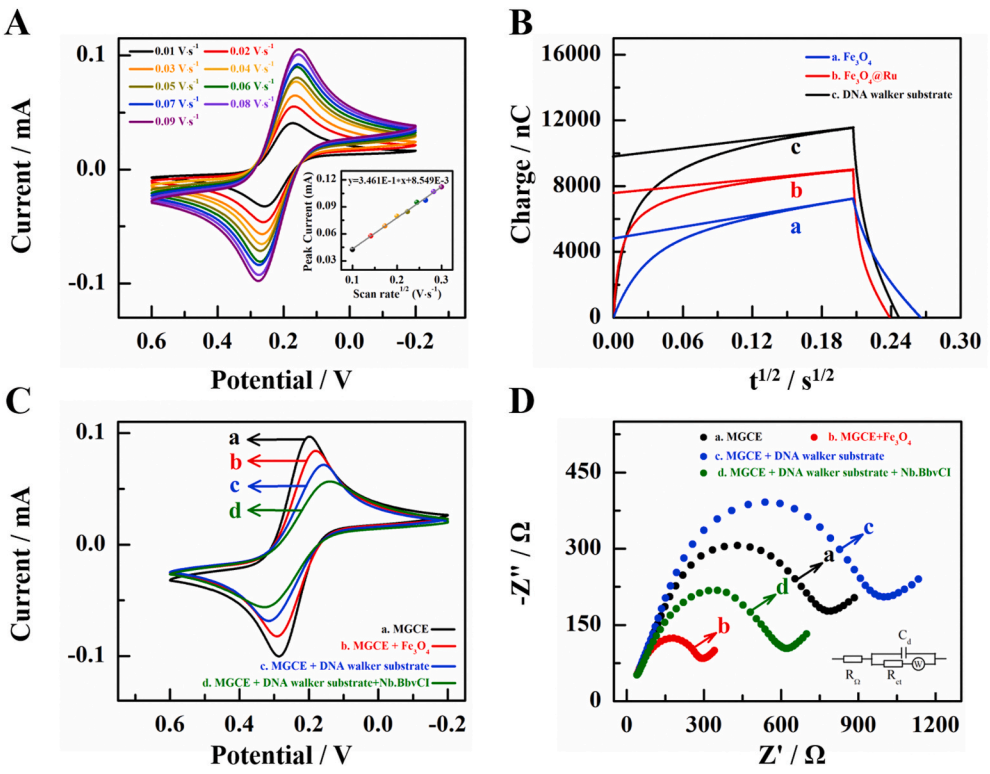

Fig. 1. Electrochemical characterization of the BTS. (A) CV curves of MGCE modified by Fe_3O_4 nanoparticles at different scan rates (0.01, 0.02, 0.03, 0.04, 0.05, 0.06, 0.07, 0.08, 0.09 $V{\cdot}s^{-1}$) in an aqueous solution containing 5 $mmol{\cdot}L^{-1}$ $K_3[Fe(CN)_6]$ and 0.1 $mol{\cdot}L^{-1}$ KCl. The inset represents the plot of CV peak current versus $v^{1/2}$. (B) CC curves of (a) Fe_3O_4, (b) Fe_3O_4@Ru and (c) DNA walker substrate in 10 $\mu mol{\cdot}L^{-1}$ Tris-HCl buffer containing 50 $\mu mol{\cdot}L^{-1}$ RuHex. The intercept ($t^{1/2} = 0$) represents the charge of RuHex diffusion (a), RuHex diffusion + Ru adsorbed on Fe_3O_4 nanoparticles (b) and RuHex diffusion + Ru adsorbed on Fe_3O_4 nanoparticles + RuHex embedded in the DNA groove (c). (C) CV and (D) EIS curves of (a) MGCE, (b) MGCE + Fe_3O_4, (c) MGCE + DNA walker substrate, and (d) MGCE + DNA walker substrate + Nb.BbvCl.

synthesized as the platform for the construction of the DNA walker substrate. The sphere diameter of Fe_3O_4 nanoparticles can be estimated as 200 ± 50 nm according to SEM images and dynamic light scattering (DLS) (Fig. S1), implying a promising electroactive surface area and DNA loading capacity. To determine the electroactive surface area, CVs of 5 $mmol{\cdot}L^{-1}$ $K_3[Fe(CN)_6]$ on MGCE adsorbed by bare Fe_3O_4 nanoparticles with same amount as the DNA walker substrate were measured at different scan rates from 0.01 to 0.09 $V{\cdot}s^{-1}$, and the linear relationship between peak current and square root of scan rate $v^{1/2}$ was analyzed (Fig. 1A). According to the Randles-Sevcik equation, the electroactive surface area of Fe_3O_4 nanoparticles on MGCE can be approximately calculated as 0.093 cm^2, large enough for subsequent DNA modification. Next, to further prove the DNA loading on the surface of Fe_3O_4 nanoparticles, zeta potential analysis was performed to analyze the modification process of the DNA walker substrate that consisted of the indicator $Ru(bpy)_2^{2+}$ and DNA walker strands including the tracker and the swing arm/blocker duplex. As shown in Fig. S1B and Fig. S2, an increased particle size and electrical property changes of the DNA walker substrate can be detected when compared with free Fe_3O_4 nanoparticles, demonstrating the reliable loading of DNA and $Ru(bpy)_2^{2+}$ on Fe_3O_4 nanoparticles. Meanwhile, the density of DNAs including the tracker and the swing arm/blocker duplex on Fe_3O_4 nanoparticles, according to Cottrell equation and Faraday's law (Anson and Osteryoung, 1983; Steel et al., 1998; Yan et al., 2018), also can be estimated to be 1.03×10^{13} $molecules{\cdot}cm^{-2}$ via CC measurement using RuHex as a redox marker (Fig. 1B). These results demonstrate that a large amount of DNA walker strands have been assembled on the surface of Fe_3O_4 nanoparticles even if the indicators $Ru(bpy)_2^{2+}$ have already occupied a part of the surface of Fe_3O_4 nanoparticles. CV and EIS were performed to test and characterize the electrochemical properties of BTS. As shown in Fig. 1C and D, compared with bare MGCE (curve a), MGCE modified with Fe_3O_4 nanoparticles presents a better conductivity and a lower charge transfer resistance R_{ct} (curve b). When the DNA walker substrate is adsorbed (curve c), the peak current decreases and R_{ct} increases due to the presence of many DNA strands. After DNA walk is initiated (curve d), the tracker strands on the BTS are hydrolyzed by Nb.BbvCI and released from the DNA walker substrate together with the blocker, resulting in an increase of peak current and a decrease of R_{ct}.

3.2. Construction of triple signal outputs mode in BTS for VP recognition

To test the feasibility of DNA walk in BTS activated by VP recognition, the stepwise DNA strands displacement reaction and the endonuclease cleavage of the DNA walker were both verified by PAGE analysis. As shown in Fig. 2A, comparing with the swing arm (lane 1) and blocker (lane 2), a new band with a slow migration rate appears to prove the formation of swing arm/blocker duplex (lane 4). As VP shows no direct effect on the DNA reaction and bands migration when involved in the DNA strand displacement reaction (Fig. S3), comparing with lane 5 and lane 6, the free substituent (lane 3) can displace the swing arm from the blocker to form the substituent/blocker duplex via the identification of VP and to form the VP/DNA complex. As shown in Fig. 2B, comparing with the swing arm (lane 1) and the hairpin tracker (lane 2), the presence of Nb.BbvCI initiates the hybridization between the swing arm and the hairpin tracker, and the cleavage to cut off the hairpin structures in the DNA walker system (lane 3 and 4). Following the principle of DNA strands displacement reaction and the DNA walk, a triple signal outputs mode can be applied to BTS. Firstly, ferrocene (Fc) modified trackers which can inhibit the ECL signals of $Ru(bpy)_2^{2+}$ are functionalized onto the surface of Fe_3O_4 nanoparticles for leading to a weak ECL "signal-1". Respectively, the FSCV signals of Fc "signal-2″ will be strong by approaching the surface of Fe_3O_4 nanoparticles. While the ECL and FSCV signals will be reversed by the VP recognition and endonuclease cleavage of tracker hairpin, which leading to turning on the "signal-1″ and turning off the "signal-2" (curve d in Fig. 2C and D). Nevertheless, signals will be maintained in the control group, because the DNA walker system has been blocked due to the lack of the target VP, substituent or Nb.BbvCI (curve a, b and c in Fig. 2C and D). Next, in the presence of VP and substituent, a VP/DNA complex will be assembled to form a duplex structure, then LC Green plus molecules that can specifically bind to the DNA double strands region and generate a strong green fluorescent signal are adopted to light up the VP/DNA complex in the supernatant

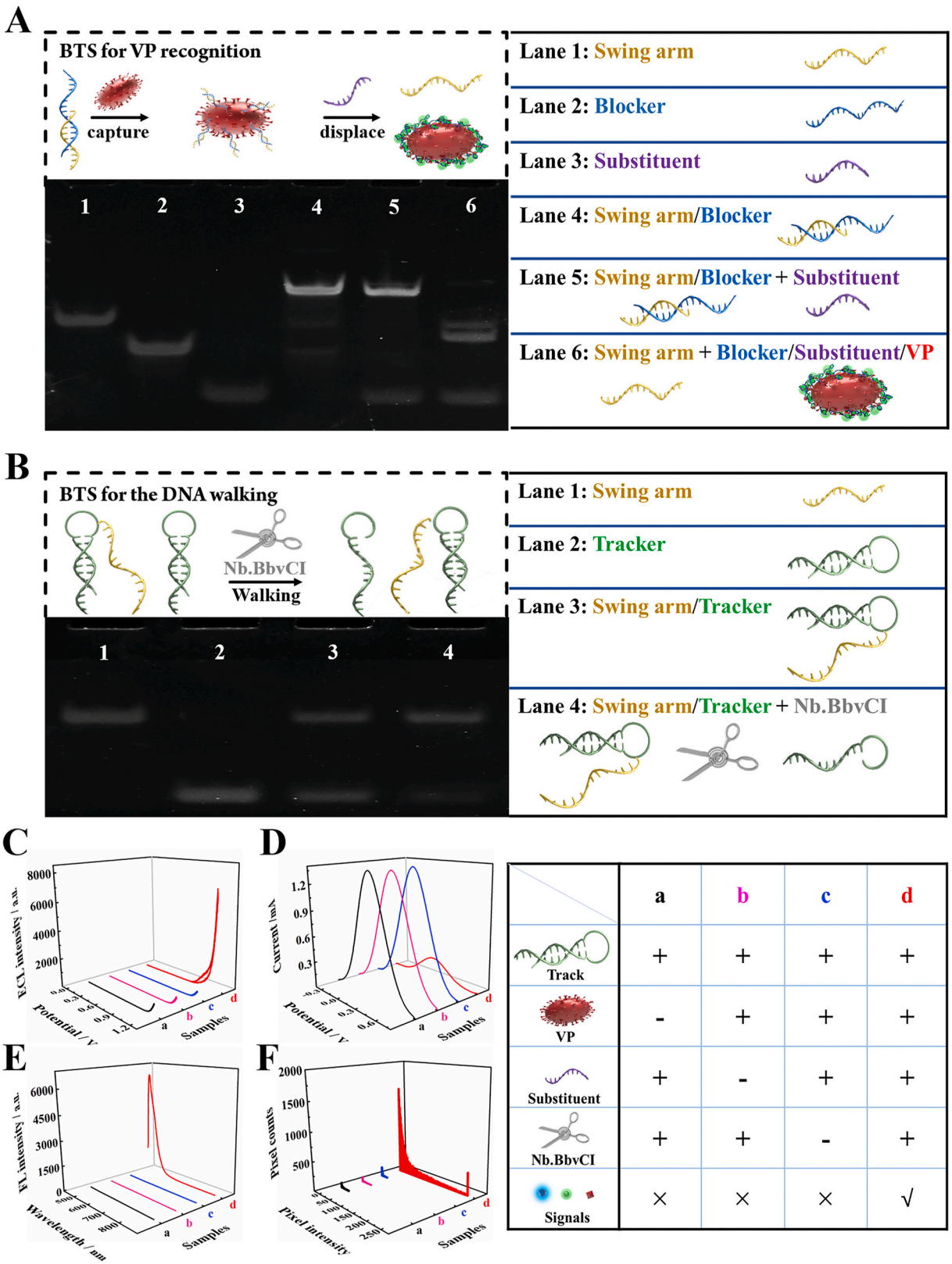

Fig. 2. The feasibility of VP recognition activated DNA walk in BTS. (A) Schematic illustration and PAGE analysis of BTS for VP recognition. (B) Schematic illustration and PAGE analysis of BTS for the DNA walking. (C) ECL, (D) FSCV, (E) FL and (F) FLPC signals of BTS without either of (a) VP, (b) substituents or (c) Nb.BbvCI, as well as with (d) all of them.

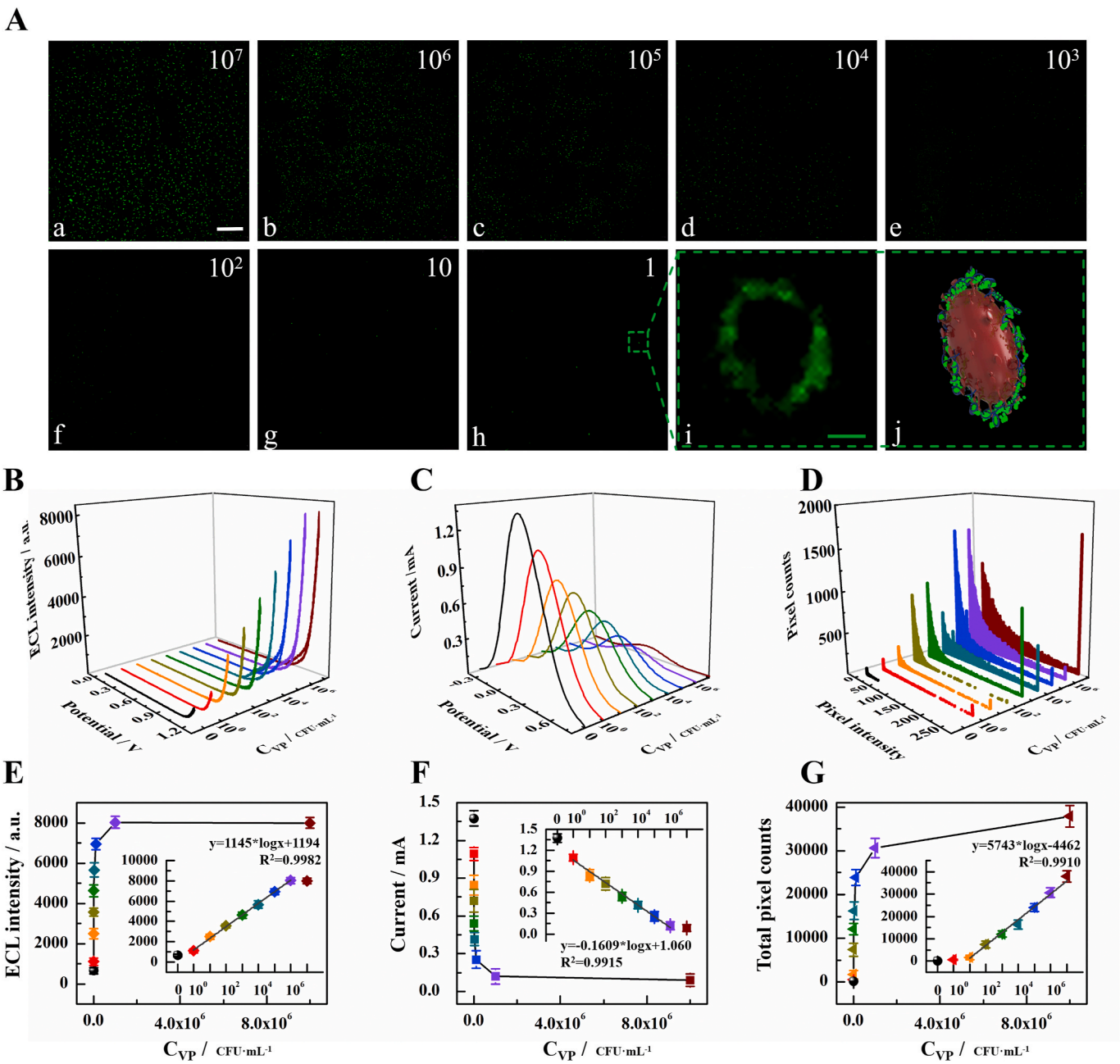

Fig. 3. Analysis of VP with triple signal outputs mode by BTS. (A) Fluorescence confocal microscope images of VP at different concentrations ranging from (a) to (h) (10^7, 10^6, 10^5, 10^4, 10^3, 10^2, 10, 1 CFU·mL^{-1}), (i) the zoom-in image of single VP and (j) the corresponding schematic image of a single VP after being captured by BTS. The scale bars are 100 μm (white) and 500 nm (green). (B) ECL, (C) FSCV and (D) FLPC signals of BTS in response to various concentrations of VP (1, 10, 10^2, 10^3, 10^4, 10^5, 10^6, 10^7 CFU·mL^{-1}). The insets represent the relationship of (E) ECL intensity (ECL), (F) current (FSCV) and (G) pixel counts (FPLC) versus VP concentrations, respectively. (For interpretation of the references to color in this figure legend, the reader is referred to the Web version of this article.)

(Fig. S3). As shown in Fig. 2E, compared with those without any one of the target VP, substituent or Nb.BbvCI (curve a, b and c), LC Green plus loaded in the tracker hairpin is induced to be released from the Fe_3O_4 nanoparticles by VP recognition and DNA walk, leading to a drastic and specific fluorescent signals enhancement after being transferred into the supernatant (curve d). FLPC method was adopted to digitize the enhanced fluorescent foci lit by the LC Green plus into pixels and then calculated by a self-made MATLAB programme (Fig. S4). Moreover, the confocal microscope imaging results can be achieved to directly image the location of VP in the supernatant by LC Green plus (Fig. S5). Collectively, the programmable and controllable DNA walker system in BTS provides a promising way for multiple-signal outputs design in corresponding to different stages of DNA walk and enables to mutually confirm the VP detection with higher reliability.

3.3. Sensitive detection and imaging of VP by BTS

With the construction of triple signal outputs mode in BTS, VP standard solutions at various concentrations (0, 1, 10, 10^2, 10^3, 10^4, 10^5, 10^6, 10^7 CFU·mL^{-1}) were quantitatively detected for five times to evaluate the sensitivity of BTS under the optimal experimental conditions (Fig. S6). ECL signals gradually increase with the increment of VP concentrations from 0 to 10^7 CFU·mL^{-1} (Fig. 3B). A good linear correlation relationship between the ECL intensity (y) and VP concentration

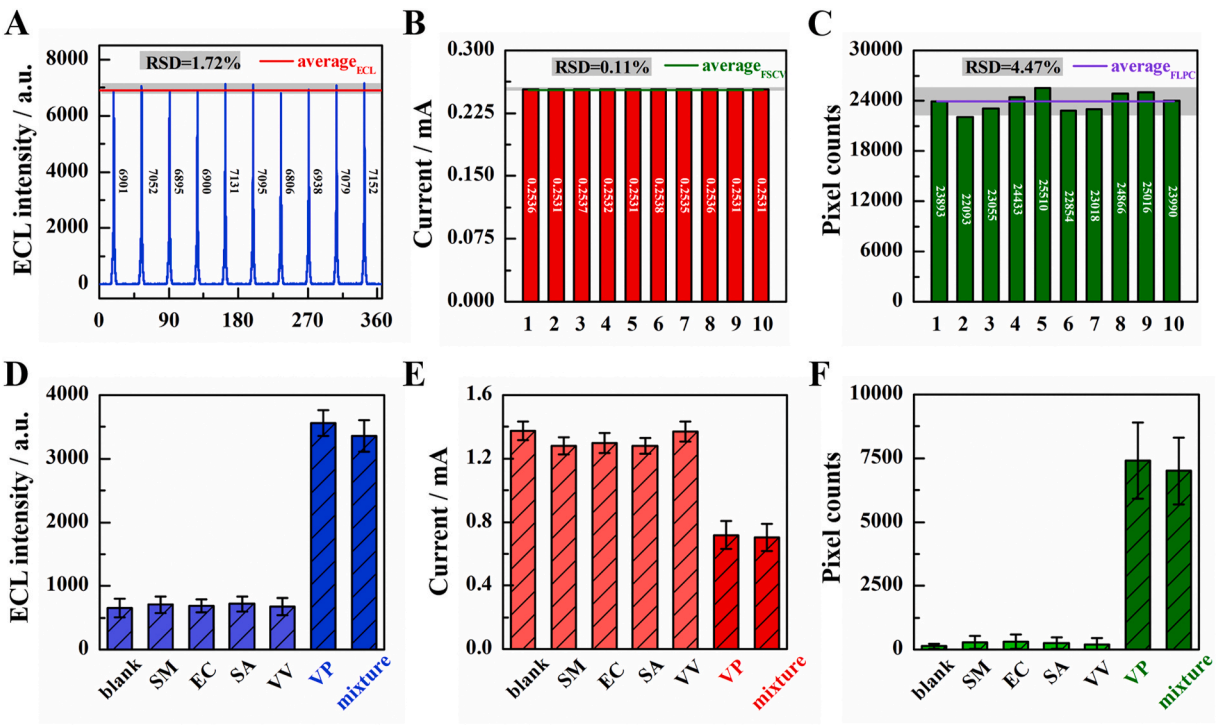

Fig. 4. Stability performance of (A) ECL, (B) FSCV and (C) FLPC signals for VP analysis by BTS. Specificity performance of (D) ECL, (E) FSCV and (F) FLPC signals for VP analysis by BTS.

(x) could be obtained from 1 to 10^6 CFU·mL^{-1}, with a linear regression equation y = 1145*logx + 1194 (R^2 = 0.9982) and a limit of quantitation of "signal-1" (LOQ1) 1 CFU·mL^{-1} (Fig. 3E). Meanwhile, as VP concentrations increase from 0 to 10^7 CFU·mL^{-1}, FSCV signals decrease correspondingly (Fig. 3C). And, there is a good linear correlation between the peak current of Fc (y) and the logarithm of VP concentration (x) ranging from 1 to 10^6 CFU·mL^{-1}. The linear regression equation is y = −0.1609*logx + 1.060 (R^2 = 0.9915), and the limit of quantitation of "signal-2" (LOQ2) is 1 CFU·mL^{-1} too (Fig. 3F). Above results show a significant improvement in detection sensitivity and detection linear range when compared with the other biosensors (Table S2). Besides, VP displays green fluorescence after being recognized by the VP aptamers and lit up by LC Green plus. As VP concentrations gradually increase from 1 to 10^7 CFU·mL^{-1}, the number of VP fluorescent foci increases respectively (Fig. 3A). Moreover, the size of a single VP could be well defined as a micron-scale detection target with a diameter of ~2 μm (Fig. 3A–i), so that it is easy to visualize and provide a legible profile of a single VP in the zoom-in image, which is also beneficial for resolving the mechanism of VP aptamer binding (Fig. 3A). In particular, every single VP is composed of multiple fluorescent foci of LC green plus and can be regarded as an aggregation of multiple unit pixels. Therefore, a math model can be established to more intuitively obtain the statistical parameters of a single VP by the FLPC method based on digital bioassay theory (Zhu et al., 2018). As a result, in each frame for VP at different concentration, the positive signal output of every LC Green plus foci can be extracted by a self-made MATLAB program based RGB (Red/-Green/Blue) color principle, and the number of green pixels ranging from 1 to 255 are equivalently counted (Fig. S4). Eventually, the relationship between the total number of the green pixels (y) and VP concentration (x) is calculated, and the linear regression equation is y = 5743*logx - 4462 (R^2 = 0.9910) as well as the LOQ in "signals-3" (LOQ3) is 10 CFU·mL^{-1} (Fig. 3D and G). Generally, LOQ1, LOQ2 and LOQ3 of triple signal outputs mode are all compatible and sensitive in pathogenic bacteria detection, indicating that the BTS enables a convincingly sensitive triple-analysis of VP.

3.4. Stable and specific detection of VP by BTS

The stability and specificity of BTS were assessed by detection of 10^5 CFU·mL^{-1} VP for ten times with different signal output modes. In 10 consecutive tests, the relative standard deviation (RSD) of ECL, FSCV and FLPC signals can be observed as 1.72% (Fig. 4A), 0.11% (Figs. 4B) and 4.47% (Fig. 4C). The three RSD results of BTS are all less than 5%, indicating the good stability of BTS in the determination of VP. To simulate the complicated bacteria environment in seawater, several different pathogenic bacteria including *Shewanella marisflavi* (SM), *Enterobacter cloacae* (EC), *Staphylococcus aureus* (SA) and *Vibrio vulnificus* (VV) at 10^6 CFU·mL^{-1}, VP at 10^2 CFU·mL^{-1} and the mixture containing 10^2 CFU·mL^{-1} of VP and 10^6 CFU·mL^{-1} of all other bacteria are chosen to investigate the specificity of BTS. As shown in Fig. 4D, E and F, compared to the detection signals of VP and VP involved mixture, the ECL, FSCV and FLPC signals in response to other non-specific pathogenic bacteria are all close to those of the blank group despite of 10000-folds concentration higher than VP, indicating the high specificity of BTS. In addition, the ECL, FSCV and FLPC signals of the VP involved mixture are approximately close to the signals of VP, which indicates the other pathogenic bacteria hardly affect the recognition of VP and reflects the excellent specificity of the BTS for VP detection. Thus, the well-developed BTS shows great performance in specifical recognition of VP in complicated real samples detection.

3.5. Precision, accuracy and consistency

To explore the detection precision and accuracy of BTS in real sample analysis, a series of VP solutions spiked in artificial seawater with different concentrations from 1 to 10^7 CFU·mL^{-1} were analyzed. As shown in Table S3, recoveries of ECL signals are 91.3%–112.5% with a RSD 4.2%–8.9%, recoveries of FSCV signals are 91.9%–118.6% with a RSD 4.8%–9.3%, and recoveries of FLPC signals are 92.5%–128.1% with a RSD 3.4%–9.7%, demonstrating the detection precision and accuracy of BTS are satisfied. The effectiveness of the triple-mode detection was verified by checking the consistency of results from ECL, FSCV and

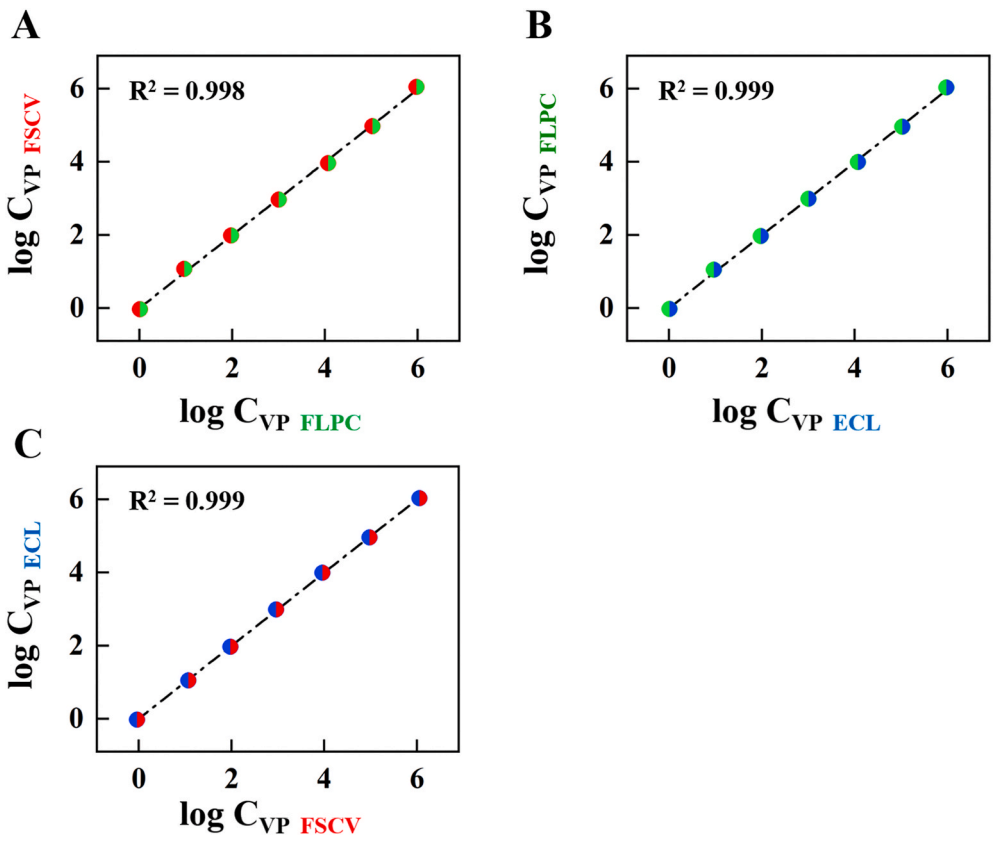

Fig. 5. Analysis of the detection correlation among the different signal outputs in BTS. The correlation curves of VP detection in real samples measured by (A) FSCV and FLPC signals, (B) FLPC and ECL signals, and (C) ECL and FSCV signals.

FLPC. It is worth mentioning that the source and nature of triple signals are different, i.e., ECL result is an optical, signal-on and electrode phase one, FSCV result is an electrochemical, signal-off and electrode phase one, and FLPC result is an optical, signal-on and solution phase one, which is conducive to the reliability of the verification. As shown in Fig. 5, the linear regression equation between FSCV (y) and FLPC (x) is $y = 0.997*x + 0.00057$ with $R^2 = 0.998$ (Fig. 5A), that between FLPC (y) and ECL (x) is $y = 0.997*x - 0.00096$ with $R^2 = 0.999$ (Fig. 5B), and that between ECL (y) and FSCV (x) is $y = 0.999*y - 0.00074$ with $R^2 = 0.999$ (Fig. 5C). In addition, inter-group *t*-test was used to check the significant difference between methods. According to the data in Table S3, the *t* value between FLPC and FSCV is 1.09, the *t* value between ECL and FLPC is 1.13, and the *t* value between FSCV and ECL is 1.11. They are all less than $t_{0.05,\ 6} = 2.45$ under the 5% significance level, proving that there is no significant difference between any two methods. The results of correlation calculation and inter-group *t*-test demonstrated the excellent consistency of the triple-mode detection.

4. Conclusion

In summary, a biosensor with triple signal outputs mode named BTS is developed for sensitive and accurate determination of VP by rationally integrating the triple signal outputs of ECL, FSCV and FLPC, which is based on the design of target-triggered DNA strand displacement reaction and aptamer recognizing. LOQs of VP were as low as 1 CFU·mL^{-1} by ECL, 1 CFU·mL^{-1} by FSCV and 10 CFU·mL^{-1} by FLPC, respectively. In addition, excellent consistency can provide a sufficient mutual verification to avoid false signals. However, this BTS relies on various large analytical equipment, which can only be performed in the laboratory at present. Our group is actively developing hand-held detection devices to enable BTS faster and more flexible analysis in food safety, water quality, and biological contamination.

CRediT authorship contribution statement

Wenting Wei: Data curation, Writing – review & editing. **Han Lin:** Data curation, Supervision, Writing – review & editing. **Tingting Hao:** Data curation. **Sui Wang:** Supervision. **Yufang Hu:** Supervision. **Zhiyong Guo:** Supervision, Conceptualization, Funding acquisition, Writing – review & editing. **Xingyu Luo:** Writing – review & editing.

Declaration of competing interest

The authors declare that they have no known competing financial interests or personal relationships that could have appeared to influence the work reported in this paper.

Acknowledgments

We gratefully acknowledge the National Natural Science Foundation of China (Grant No. 42076193, 41576098), and Ningbo Science and Technology Bureau (202002N3061). This work was also sponsored by K. C. Wong Magna Fund at Ningbo University.

Appendix A. Supplementary data

Supplementary data to this article can be found online at https://doi.org/10.1016/j.bios.2021.113305.

References

Anson, F.C., Osteryoung, R.A., 1983. J. Chem. Educ. 60 (4), 293–296.
Azizi, M., Zaferani, M., Cheong, S.H., Abbaspourrad, A., 2019. ACS Sens. 4 (4), 841–848.
Bath, J., Turberfield, A.J., 2007. Nat. Nanotechnol. 2 (5), 275–284.
Bazrafshan, A., Meyer, T.A., Su, H., Brockman, J.M., Blanchard, A.T., Piranej, S., Duan, Y., Ke, Y., Salaita, K., 2020. Angew. Chem. Int. Ed. 59 (24), 9514–9521.

Charlermroj, R., Himananto, O., Seepiban, C., Kumpoosiri, M., Warin, N., Gajanandana, O., Elliott, C.T., Karoonuthaisiri, N., 2014. Anal. Chem. 86 (14), 7049–7056.
Chen, G., Xie, J., Zhang, Z., Meng, W., Zhang, C., Kang, K., Wu, Y., Guo, Z., 2019. Sensor. Actuator. B Chem. 301, 127135.
Chen, J., Andler, S.M., Goddard, J.M., Nugen, S.R., Rotello, V.M., 2017. Chem. Soc. Rev. 46 (5), 1272–1283.
Costa, T.R., Felisberto-Rodrigues, C., Meir, A., Prevost, M.S., Redzej, A., Trokter, M., Waksman, G., 2015. Nat. Rev. Microbiol. 13 (6), 343–359.
Gahlaut, S.K., Kalyani, N., Sharan, C., Mishra, P., Singh, J.P., 2019. Biosens. Bioelectron. 126, 478–484.
Guo, Z., Jia, Y., Song, X., Lu, J., Lu, X., Liu, B., Han, J., Huang, Y., Zhang, J., Chen, T., 2018. Anal. Chem. 90 (10), 6124–6130.
Hao, Z., Lin, X., Li, J., Yin, Y., Gao, X., Wang, S., Liu, Y., 2020. Biosens. Bioelectron. 173, 112789.
Hillman, Y., Gershberg, J., Lustiger, D., Even, D., Braverman, D., Dror, Y., Ashur, I., Vernick, S., Sal-Man, N., Wine, Y., 2021. Anal. Chem. 93 (2), 928–935.
Hu, Q., Li, H., Wang, L., Gu, H., Fan, C., 2019. Chem. Rev. 119 (10), 6459–6506.
Hu, Y., Wang, Y., Yan, J., Wen, N., Xiong, H., Cai, S., He, Q., Peng, D., Liu, Z., Liu, Y., 2020. Adv. Sci. 7 (14), 2000557.
Kannan, P., Chen, J., Su, F., Guo, Z., Huang, Y., 2019. Anal. Chem. 91 (23), 14792–14802.
Li, S., Xu, L., Ma, W., Wu, X., Sun, M., Kuang, H., Wang, L., Kotov, N.A., Xu, C., 2016. J. Am. Chem. Soc. 138 (1), 306–312.
Liang, C.P., Ma, P.Q., Liu, H., Guo, X., Yin, B.C., Ye, B.C., 2017. Angew. Chem. Int. Ed. 56 (31), 9077–9081.
Lv, H., Chen, A., Cheng, W., Kong, L., Zhao, M., Ding, S., Ju, H., Cheng, W., 2020. Anal. Chem. 92 (23), 15624–15631.
Ma, C., Cao, Y., Gou, X., Zhu, J.J., 2020. Anal. Chem. 92 (1), 431–454.
Mason, S.D., Tang, Y., Li, Y., Xie, X., Li, F., 2018. TrAC Trends Anal. Chem. (Reference Ed.) 107, 212–221.
Pan, J., Cha, T.G., Li, F., Chen, H., Bragg, N.A., Choi, J.H., 2017. Sci. Adv. 3 (1), e1601600.
Peleg, A.Y., Hooper, D.C., 2010. N. Engl. J. Med. 362 (19), 1804–1813.
Shao, H., Lin, H., Guo, Z., Lu, J., Jia, Y., Ye, M., Su, F., Niu, L., Kang, W., Wang, S., Hu, Y., Huang, Y., 2019. Biosens. Bioelectron. 143, 111616.
Smith, B.R., Gambhir, S.S., 2017. Chem. Rev. 117 (3), 901–986.
Steel, A.B., Herne, T.M., Tarlov, M.J., 1998. Anal. Chem. 70 (22), 4670–4677.
Su, Y.C., Liu, C., 2007. Food Microbiol. 24 (6), 549–558.
Tagit, O., Hildebrandt, N., 2017. ACS Sens. 2 (1), 31–45.
Tlili, C., Sokullu, E., Safavieh, M., Tolba, M., Ahmed, M.U., Zourob, M., 2013. Anal. Chem. 85 (10), 4893–4901.
Wang, D., Vietz, C., Schroder, T., Acuna, G., Lalkens, B., Tinnefeld, P., 2017. Nano Lett. 17 (9), 5368–5374.
Wang, D., Yu, L., Huang, C.-M., Arya, G., Chang, S., Ke, Y., 2021. J. Am. Chem. Soc. 143 (5), 2256–2263.
Wang, F., Liu, X., Willner, I., 2015. Angew. Chem. Int. Ed. 54 (4), 1098–1129.
Wang, Q., Wang, T., Lin, H., Meng, W., Zhang, C., Cai, P., Hao, T., Wu, Y., Guo, Z., 2020a. Sensor. Actuator. B Chem. 320, 128349.
Wang, T., Lin, H., Wu, Y., Guo, Z., Hao, T., Hu, Y., Wang, S., Huang, Y., Su, X., 2020b. Biosens. Bioelectron. 163, 112277.
Wei, W., Lin, H., Shao, H., Hao, T., Wang, S., Hu, Y., Guo, Z., Su, X., 2020. Microchim. Acta 187 (9), 529.
Xiong, Y., Zhang, J., Yang, Z., Mou, Q., Ma, Y., Xiong, Y., Lu, Y., 2020. J. Am. Chem. Soc. 142 (1), 207–213.
Yan, T., Zhu, L., Ju, H., Lei, J., 2018. Anal. Chem. 90 (24), 14493–14499.
Yeung, P.S., Boor, K.J., 2004. Foodb. Pathog. Dis. 1 (2), 74–88.
Yoo, S.M., Lee, S.Y., 2016. Trends Biotechnol. 34 (1), 7–25.
Zhang, L., Orth, K., 2013. Curr. Opin. Microbiol. 16 (1), 70–77.
Zhang, N., Ye, S., Wang, Z., Li, R., Wang, M., 2019. ACS Sens. 4 (4), 924–930.
Zhou, L., Gao, M., Fu, W., Wang, Y., Luo, D., Chang, K., Chen, M., Chen, M., Chen, M., 2020. Sci. Adv. 6 (22), eabb0695.
Zhu, L., Liu, Q., Yang, B., Ju, H., Lei, J., 2018. Anal. Chem. 90 (11), 6357–6361.